Research Article

Battery Energy Storage System for PV Output Power Leveling

Rajkiran Singh, Seyedfoad Taghizadeh, Nadia Mei Lin Tan, and Jagadeesh Pasupuleti

Department of Electrical Power Engineering, Universiti Tenaga Nasional, Jalan IKRAM-UNITEN, 43000 Kajang, Selangor, Malaysia

Correspondence should be addressed to Nadia Mei Lin Tan; nadia@uniten.edu.my

Fluctuating photovoltaic (PV) output power reduces the reliability in power system when there is a massive penetration of PV generators. Energy storage systems that are connected to the PV generators using bidirectional isolated dc-dc converter can be utilized for compensating the fluctuating PV power. This paper presents a grid connected energy storage system based on a 2 kW full-bridge bidirectional isolated dc-dc converter and a PWM converter for PV output power leveling. This paper proposes two controllers: a current controller using the d-q synchronous reference and a phase-shift controller. The main function of the current controller is to regulate the voltage at the high-side dc, so that the voltage ratio of the high-voltage side (HVS) with low-voltage side (LVS) is equal to the transformer turns ratio. The phase-shift controller is employed to manage the charging and discharging modes of the battery based on PV output power and battery voltage. With the proposed system, unity power factor and efficient active power injection are achieved. The feasibility of the proposed control system is investigated using PSCAD simulation.

1. Introduction

Many countries are implementing PV solar panels as they are a clean and sustainable source to meet their power demands. However, the grid connected PV unit without energy storage unit can affect the utility grid in a negative manner due to the intermittent nature of PV. In order to solve this problem, integration of energy storage system to level the output power of PV is necessary [1–4].

There are many types of energy storage systems such as superconducting magnetic energy storage, flywheel, capacitor, battery, and pump hydrostorage. The battery energy storage device is modular, making it easy to be connected close to the point of load and the PV generators. Li-ion batteries have high energy density and are being increasingly used in battery connected PV systems [5]. However, as long as it is employed for PV application, an efficient bidirectional system is required to perform the charging and discharging of the batteries.

Various configuration of a bidirectional isolated dc-dc converter has been investigated in [6]. Bidirectional dc-dc converter can be categorized as isolated and nonisolated topologies. Although an isolated converter is more complicated and expensive than a nonisolated converter, it benefits the system safety, reliability, and flexibility. In addition, the full-bridge topology has a high efficiency, while providing minimum switching loss, improved EMI, and galvanic isolation for energy storage systems. It is also preferred due to its minimal voltage and current stress in high-power applications [7–9]. The bidirectional full-bridge isolated dc-dc converter is a reliable system with high efficiency for PV applications in order to remove probable fluctuations and stabilize the PV output.

As Figure 1 shows, typically, a battery energy storage system (BESS) consists of a battery bank, a bidirectional full-bridge isolated dc-dc converter, and a grid connected PWM converter. In addition to the power circuit of the converters, a reliable control system is required for two main purposes. Firstly, it is to manage the power flow in both directions, achieving charging and discharging modes of the battery. Secondly, it is to adjust the voltage of HVS with respect to the voltage of LVS of the converter so that the voltage ratio of the HVS with LVS is close to the transformer turns ratio [10]. The voltage adjustment is necessary to decrease the peak switching current and the turn-off overvoltage across the semiconductor switches.

A 6 kW bidirectional isolated dc-dc converter connecting a Li-ion battery bank to the utility grid via a PWM converter
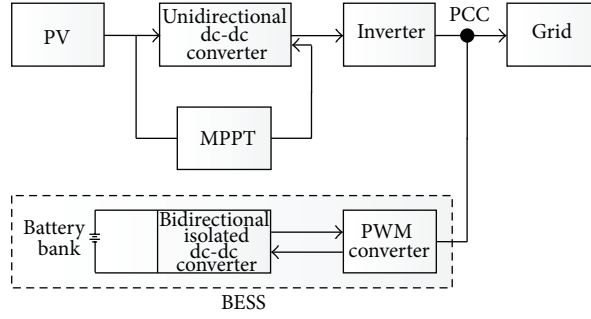
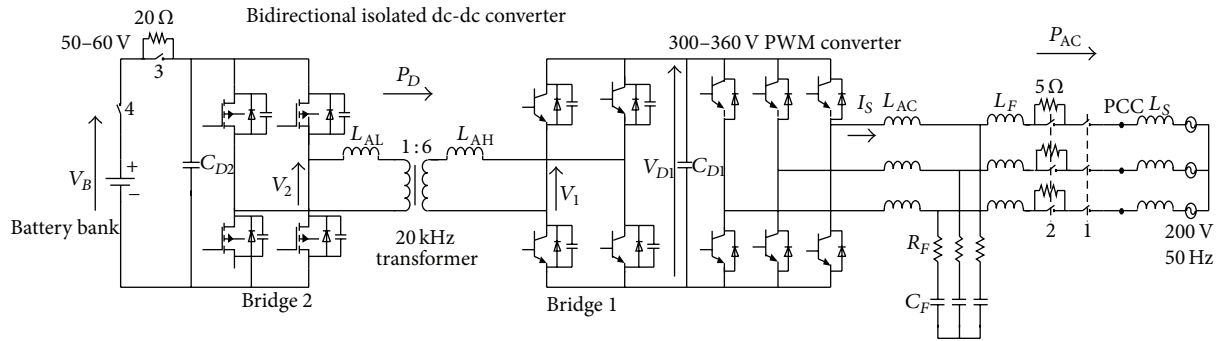FIGURE 1: Battery energy storage and PV systems connected to the utility grid.

FIGURE 2: The grid-connected BESS based on a bidirectional isolated dc-dc converter. L_S is the background system impedance. $L_{AC} = 280\,\mu$H (0.4%), $L_F = 44\,\mu$H (0.1%), $R_F = 0.2\,\Omega$ (1%), and $C_F = 150\,\mu$F, on a three-phase 200 V, 2 kW, and 50 Hz base.

has been presented in [10, 11]. The paper in [11] mitigated the effects of the dc-bias currents in the high frequency transformer through the design of an air gap in the transformer. The control method employed is feed-forward phase-shift modulation with no online voltage regulation of the HVS. Hence, the voltage ratio of the HVS with LVS was manually controlled so that it is close to the transformer turns ratio.

This paper focuses on the overall control of the BESS which includes the controls of the bidirectional isolated dc-dc converter and the PWM converter. This paper proposes two controllers for the BESS. The first part is a feedback controller that regulates the voltage of HVS DC capacitor based on the battery bank voltage and the second part determines the direction and the amount of the required BESS power based on the PV output power and battery bank voltage. Accordingly, while the 2 kW bidirectional isolated dc-dc converter operates to regulate the power at the PCC, the proposed control system continuously adjusts the voltages of HVS so that the voltage ratio of the HVS with LVS is close to the transformer turns ratio, resulting in increasing the converter efficiency. This paper verifies the proposed BESS for the application of PV output power leveling via simulation in PSCAD.

2. Power Circuit Configuration

Figure 2 shows the battery bank connected at the low-voltage side (LVS) of the 2 kW dc-dc converter. The PWM converter

TABLE 1: Circuit parameters of the bidirectional isolated dc-dc converter.

Rated power	P_{DC}	2 kW
Transformer turns ratio	$N:1$	6 : 1
Auxiliary inductor (HVS)	L_{AH}	80 μH (15.5%)
Snubber capacitor (HVS)	C_{SH}	10 nF
DC capacitor (HVS)	C_{D1}	1 mF
Auxiliary inductor (LVS)	L_{AL}	3.5 μH (24.4%)
Snubber capacitor (LVS)	C_{SL}	150 nF
DC capacitor (LVS)	C_{D2}	1 mF
Switching frequency	f	20 kHz

HVS is based on 2 kW, 360 V, and 20 kHz.
LVS is based on 2 kW, 60 V, and 20 kHz.

interfaces the high-voltage side (HVS) of the dc-dc converter with the utility grid at the PCC via the switching ripple filters and AC inductors. A 20 kHz high frequency transformer with a turns ratio of 6 : 1 is utilized as it is small in size and light in weight. It also provides galvanic isolation to ensure system safety and reliability. The circuit configuration is similar to that in [10]. However, this paper investigates the feasibility of the system in PV output power leveling via the proposed control system.

Table 1 summarizes the parameters of the circuit in Figure 2. The operating voltage of the battery, V_B, is set between 50 V and 60 V and at the high-voltage side, V_{D1} is
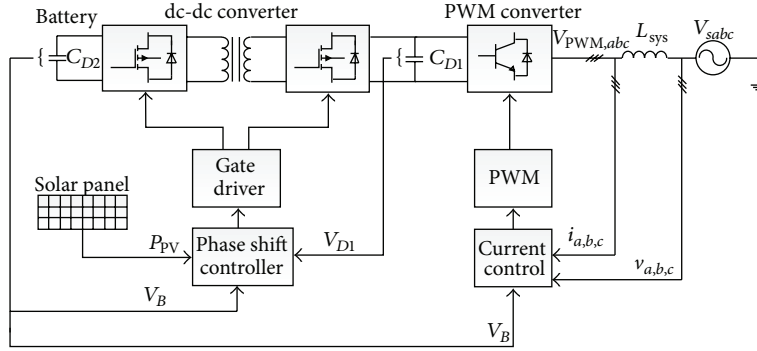
FIGURE 3: Configuration of the proposed control system.

TABLE 2: The gains of the three PI controllers.

	PI_1	PI_2	PI_3
Proportional gain K_p	0.5	0.48	0.9
Integral gain K_I	0.03	0.25	0.04

regulated between 300 V and 360 V to maintain the ratio of HVS and LVS close to the transformer turns ratio. The rated voltage of 60 V is selected taking into consideration user safety. The minimum voltage of 60 V is based on the specification of Li-ion battery available. The BESS is sized for active power injection at the PCC of up to 2 kW. The power transfer, P_D, of the bidirectional isolated dc-dc converter can easily be controlled by adjusting the phase-shift angle δ between two AC voltages V_1 and V_2 as expressed as [12]

$$P_D = \frac{V_{D1}V_B}{\omega L}\delta\left(1 - \frac{|\delta|}{\pi}\right), \tag{1}$$

where V_{D1} is the high-side voltage, V_B is the battery voltage at the low-voltage side, ω is the angular switching frequency, and L is the sum of the transformer leakage and auxiliary inductance referred to as the high-voltage side. In a practical system, the leakage inductance of the high-frequency transformer should be minimized to prevent the so-called spot heating on the transformer. In the simulation system, the leakage inductance of the transformer is neglected.

A start-up circuit, consisting of four circuit breakers, is employed to prevent a large inrush current flow into the dc capacitors, which will result in saturating the AC inductors in a practical system. Therefore, the start-up procedure is employed to charge capacitors C_{D1} and C_{D2} through 5 Ω and 20 Ω resistors connected on the utility and battery sides, respectively.

3. Overall Control System

Figure 3 presents the proposed overall control system. The proposed control system regulates the injected power at the PCC to be at 2 kW. The current control technique has been employed to regulate the voltage across dc-link capacitor C_{D1}. Three-phase d-q axis transformation control strategy

is employed to regulate the capacitor voltage of the PWM converter, V_{D1}, based on the battery voltage V_B. In fact, this system monitors V_B and keeps V_{D1} at a level where the voltage ratio between V_{D1} and V_B is close to the transformer turns ratio. On the other hand, the phase shift controller considers output power of PV, P_{PV}, to determine the desired output power from the BESS such that

$$P_{BESS} = P_{PCC} - P_{PV}, \tag{2}$$

where in this paper P_{PCC} = 2 kW. The controller also considers the battery voltage, V_B, and the HVS capacitor voltage, V_{D1}. Then it calculates the new phase shift angle, δ, needed to level the PV output power through battery charging or discharging. Note that for the purpose of simulation, the PV output power is assumed and the modelling of PV generation system is outside the scope of this paper.

Figure 4 shows the verification flow chart of the power management system of the phase-shift controller in the battery energy storage system. The amount of active power required to compensate the PV output power is calculated by the phase-shift controller. Three PV output power conditions are considered during the operation of the proposed control system. In the first condition, the output power of PV is less than 2 kW. The controller checks the battery voltage to be between 50 V and 60 V (50 V < V_B ≤ 60 V). Then the BESS operates in the discharging mode to compensate for the reduced PV output power. In the second condition, the output power of PV is 2 kW. In this case BESS goes to standby mode by changing the phase shift to zero. In the third condition, the output power of PV is more than 2 kW. The controller checks the battery voltage to be less than 60 V (V_B < 60 V). Then the BESS is charged to absorb the surplus power of PV. As shown in Figure 4, there are two other conditions where the BESS goes on standby mode:

(i) when the battery voltage is less than 50 V and the P_{PV} is less than 2 kW,

(ii) when the battery voltage is more than 60 V and the P_{PV} is more than 2 kW.

This is to protect the Li-ion battery bank from being overcharged and over discharged [13]. Apart from putting the BESS on standby, the excess power of PV can be discharged through a dump load [14].
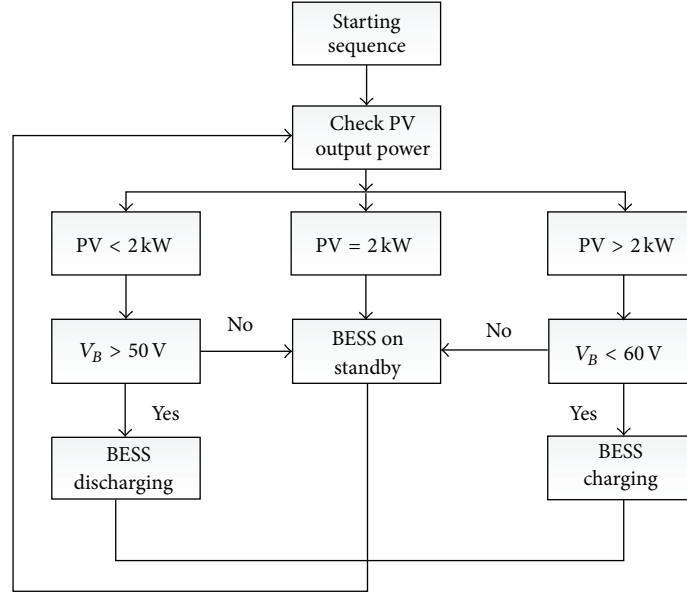
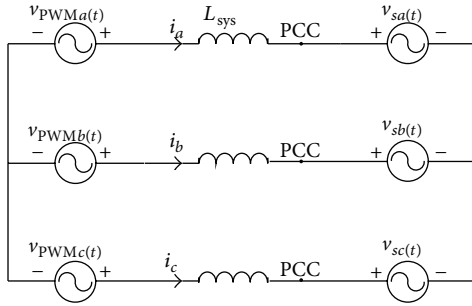FIGURE 4: The verification flow chart to ascertain the BESS to be in standby, charging, or discharging mode.

FIGURE 5: Equivalent circuit of the proposed system.

3.1. Control Algorithm of PWM Converter. Figure 5 illustrates the equivalent circuit of PWM converter and grid. The proposed control system regulates the three phase currents, i_a, i_b, and i_c to achieve unity power factor and to regulate the dc-link voltage at the PWM converter. A PLL has been employed for providing the grid phase angle information, ωt. The PLL provides fast and accurate synchronization information with a high degree of immunity and insensitivity to disturbances, harmonics, unbalances, sags/swells, notches, and other types of distortions in the input signal. An accurate estimation of utility phase angle is critical for maintaining the power quality at the PCC. The Kirchhoff voltage law (KVL) can be applied to Figure 5, and the three-phase KVL equation is expressed as

$$L_{\text{sys}} \frac{d}{dt} \begin{bmatrix} i_a \\ i_b \\ i_c \end{bmatrix} = \begin{bmatrix} v_{sa} \\ v_{sb} \\ v_{sc} \end{bmatrix} - \begin{bmatrix} v_{\text{PWM}a} \\ v_{\text{PWM}b} \\ v_{\text{PWM}c} \end{bmatrix}, \tag{3}$$

where v_s is the three-phase voltage at the PCC, L_{sys} ($L_{\text{AC}} + L_F + L_S$) is the total per phase series inductance, and v_{PWM}

is the three-phase output voltage of the PWM converter. The supply voltage can be defined as

$$\begin{bmatrix} v_{sa} \\ v_{sb} \\ v_{sc} \end{bmatrix} = \widehat{V} \begin{bmatrix} \cos \omega t \\ \cos (\omega t - \theta) \\ \cos (\omega t + \theta) \end{bmatrix}, \tag{4}$$

where $\widehat{V}$ is the magnitude of the voltage at the PCC, ωt is the phase angle, and θ is $2\pi/3$ for a balanced three-phase system. The proposed control system is based on the d-q transformation method. The d and q components of the three-phase current i_a, i_b, and i_c are obtained using Park's transformation through the transformation matrix,

$$P = \frac{2}{3} \begin{bmatrix} \cos \omega t & \cos \left(\omega t - \dfrac{2\pi}{3} \right) & \cos \left(\omega t + \dfrac{2\pi}{3} \right) \\ \sin \omega t & \sin \left(\omega t - \dfrac{2\pi}{3} \right) & \sin \left(\omega t + \dfrac{2\pi}{3} \right) \\ \dfrac{1}{2} & \dfrac{1}{2} & \dfrac{1}{2} \end{bmatrix}. \tag{5}$$

The inverse of the Park's transformation matrix is defined as

$$P^{-1} = \begin{bmatrix} \cos \omega t & \sin \omega t & 1 \\ \cos \left(\omega t - \dfrac{2\pi}{3} \right) & \sin \left(\omega t - \dfrac{2\pi}{3} \right) & 1 \\ \cos \left(\omega t + \dfrac{2\pi}{3} \right) & \sin \left(\omega t + \dfrac{2\pi}{3} \right) & 1 \end{bmatrix}. \tag{6}$$

Using (5) and (6), equation (3) can be rewritten as

$$P * L_{\text{sys}} * \frac{d}{dt} P^{-1} \begin{bmatrix} I_d \\ I_q \\ I_0 \end{bmatrix} = PP^{-1} \begin{bmatrix} V_{sd} \\ V_{sq} \\ V_{s0} \end{bmatrix} - PP^{-1} \begin{bmatrix} V_{\text{PWM}d} \\ V_{\text{PWM}q} \\ V_{\text{PWM}0} \end{bmatrix}. \tag{7}$$
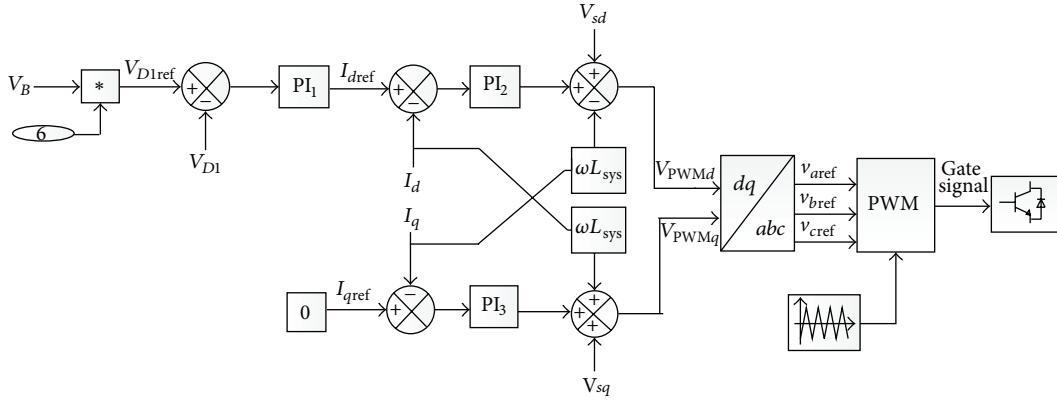
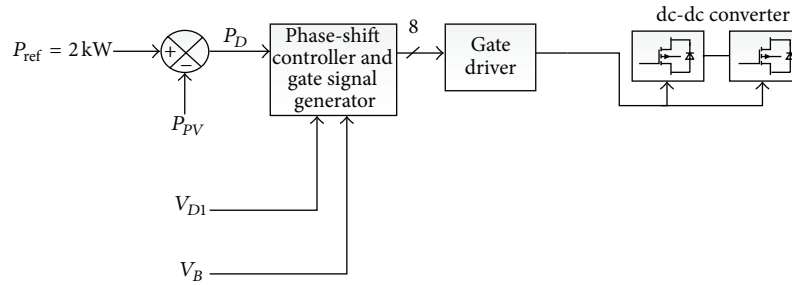Figure 6: Current control of the PWM converter.

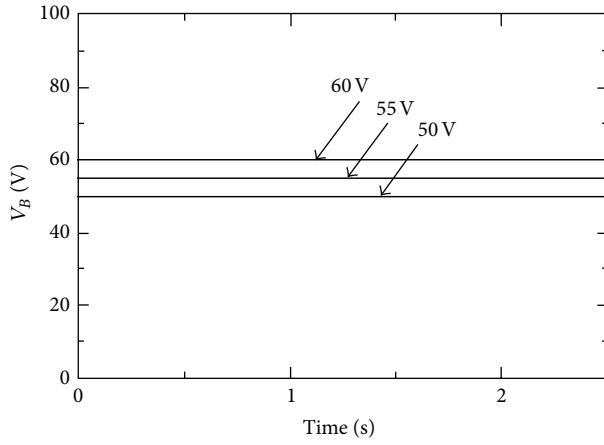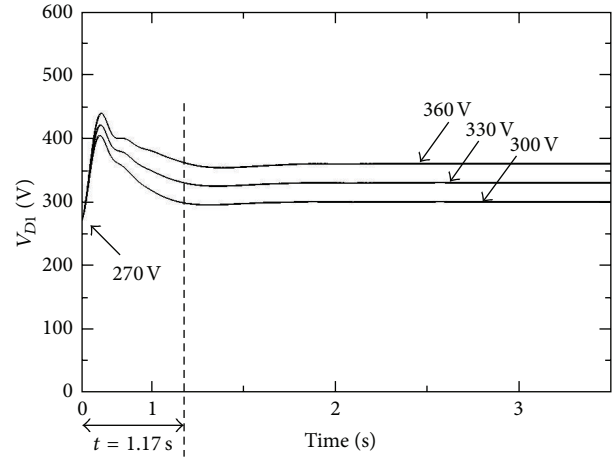Figure 7: Phase shift angle control of the bidirectional isolated dc-dc.

Figure 8: Battery voltage at 50 V, 55 V, and 60 V.

Figure 9: The HVS capacitor voltage, V_{D1}, regulated at 300 V, 330 V, and 360 V.

In a balance system, the zero sequence component is equivalent to zero and can be omitted, resulting in

$$\frac{d}{dt}\begin{bmatrix} I_d \\ I_q \end{bmatrix} = \begin{bmatrix} 0 & -\omega \\ \omega & 0 \end{bmatrix}\begin{bmatrix} I_d \\ I_q \end{bmatrix} + \begin{bmatrix} \dfrac{1}{L_{\text{sys}}} & 0 \\ 0 & \dfrac{1}{L_{\text{sys}}} \end{bmatrix}\begin{bmatrix} V_{sd} \\ V_{sq} \end{bmatrix}$$
$$- \begin{bmatrix} \dfrac{1}{L_{\text{sys}}} & 0 \\ 0 & \dfrac{1}{L_{\text{sys}}} \end{bmatrix}\begin{bmatrix} V_{\text{PWM}d} \\ V_{\text{PWM}q} \end{bmatrix}. \tag{8}$$

Equation (8) can be divided into

$$\frac{dI_d}{dt} = -\omega I_q + \frac{V_{sd}}{L_{\text{sys}}} - \frac{V_{\text{PWM}d}}{L_{\text{sys}}},$$
$$\frac{dI_q}{dt} = \omega I_d + \frac{V_{sq}}{L_{\text{sys}}} - \frac{V_{\text{PWM}q}}{L_{\text{sys}}}. \tag{9}$$
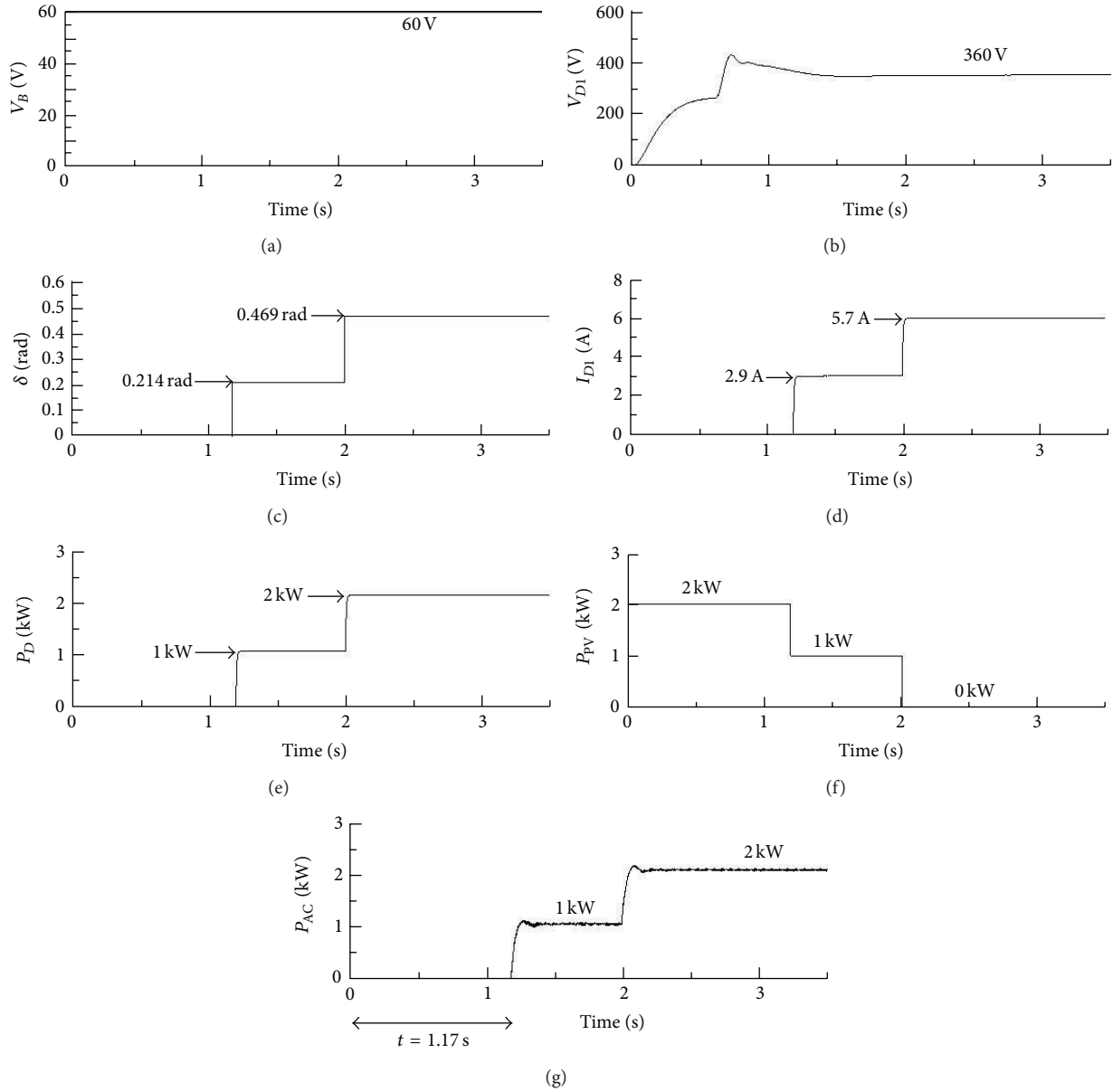
(a)

(b)

(c)

(d)

(e)

(f)

(g)

FIGURE 10: Simulation waveforms of the step PV output change from 2 kW to 0 kW. (a) Battery voltage. (b) High-voltage-side capacitor voltage. (c) Phase-shift angle. (d) High-side dc current. (e) BESS DC power. (f) PV output power. (g) BESS AC output power.

The steady-state condition is achieved when the derivative terms of dI_d/dt and dI_q/dt are equal to zero. Then $V_{\text{PWM}d}$ and $V_{\text{PWM}q}$ can be obtained as

$$V_{\text{PWM}d} = -\omega L_{\text{sys}} I_q + V_{sd},$$
$$V_{\text{PWM}q} = \omega L_{\text{sys}} I_d + V_{sq}. \tag{10}$$

Equations (10) are implemented as part of the control in Figure 6. The goal of the control system is to regulate the voltage of HVS dc-link capacitor, V_{D1}, by controlling the line currents, i_a, i_b, and i_c. To generate the reference direct component of current, $I_{d\text{ref}}$, the instantaneous battery voltage V_B is multiplied by the transformer turns ratio and is compared with the HVS capacitor voltage V_{D1}. Then the error is passed

through a proportional-integral controller, PI$_1$. Therefore, the reference direct component of current is calculated as

$$I_{d\text{ref}} = \{V_{D1\text{ref}} - V_{D1}\} \left(K_{P1} + \int K_{I1} d_t \right). \tag{11}$$

The quadrature reference current, $I_{q\text{ref}}$ is set at zero to avoid any reactive power transfer. These two references are compared with the actual values of I_d and I_q and the differences are passed through two PI controllers, PI$_2$ and PI$_3$. The outputs of PI controllers are added with measured V_{sd} and V_{sq}, based on (10) for achieving $V_{\text{PWM}d}$ and $V_{\text{PWM}q}$. The proportional-integral controllers PI$_2$ and PI$_3$ transform
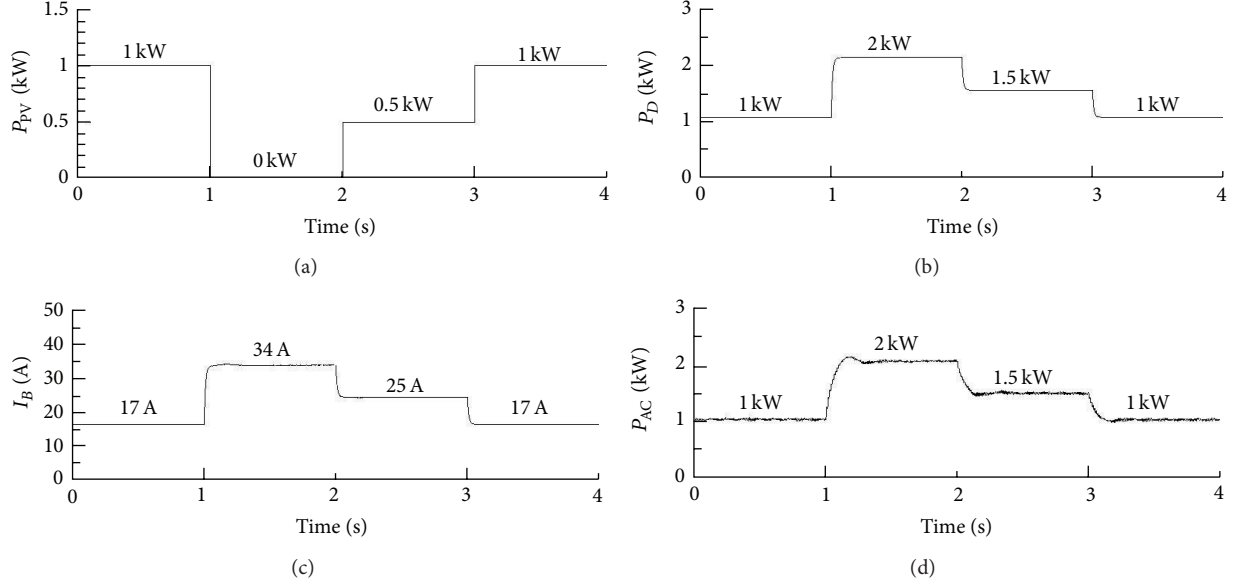
FIGURE 11: BESS response at $V_B = 55$ V. (a) PV output power. (b) BESS DC power. (c) Battery current. (d) BESS AC output power.

the errors from the comparisons of d-q components of current into voltage value as

$$
\begin{aligned}
V_{\text{PWM}d} &= \left\{ I_{d\text{ref}} - I_d \right\} \left(K_{p2} + \frac{K_{I2}}{s} \right) - \omega L_{\text{sys}} I_q + V_{sd}, \\
V_{\text{PWM}q} &= \left\{ 0 - I_q \right\} \left(K_{p3} + \frac{K_{I3}}{s} \right) + \omega L_{\text{sys}} I_d + V_{sq},
\end{aligned}
\tag{12}
$$

where V_{sd} is the measured magnitude of the grid voltage and V_{sq} is almost zero. The gain from ωL_{sys} is considered to provide the decoupling terms. The parameters K_p and K_I are tuned by trial and error method. Table 2 presents the parameter of each PI controller. Finally, the dq reference voltages are transformed to $v_{a\text{ref}}$, $v_{b\text{ref}}$, and $v_{c\text{ref}}$ which are the sinusoidal reference voltages of the PWM generator.

3.2. Control Algorithm of the Bidirectional Isolated dc-dc Converter.
Figure 7 shows the control system of the bidirectional isolated dc-dc converter. The battery is charged or discharged through the bidirectional isolated dc-dc converter connected to the PWM converter. Based on this concept, the control system determines the desired BESS power as in (2) in order to regulate the injected power at the PCC at 2 kW as the PV output power varies. The battery power is assumed to be equal to the power transfer P_D. The measured values of P_{PV}, V_{D1}, and V_B are employed to compute the phase-shift angle δ for the required battery charging power as

$$
\delta = \frac{\pi}{2} - \sqrt{\frac{\pi^2}{4} - \frac{\omega \pi L P_D}{V_{D1} V_B N}}
\tag{13}
$$

TABLE 3: Breaker operations during startup.

HVS dc-link capacitor voltage	Breaker 1	Breaker 2	Breaker 3	Breaker 4
$V_{D2} < 270$ V	Close	Open	Open	Close
270 V $\leq V_{D2} < 360$ V	Close	Close	Open	Close
$V_{D2} = 360$ V	Close	Close	Close	Close

and the phase-shift angle for the required battery discharging power as

$$
\delta = -\frac{\pi}{2} + \sqrt{\frac{\pi^2}{4} + \frac{\omega \pi L P_D}{V_{D1} V_B N}}.
\tag{14}
$$

In the phase-shift controller block, it generates 8 gate signals for the gate driver. The gate driver amplifies the signals and sends it to the full bridge converter.

3.3. Simulation Method.
A simulation model with the control system is built using PSCAD based on Figures 2 and 3. The circuit parameters and gains in Tables 1 and 2 are used, respectively. The rated output power of the BESS is 2 kW, for a PV generation system rated at 2 kW. The rms voltage of the grid is 200 V and its rated frequency is 50 Hz. The switching frequency of the PWM converter is 10 kHz and for the bidirectional isolated dc-dc converter it is 20 kHz. The simulation duration is 3.5 s and the time step is 0.3 μs.

Table 3 shows the operating sequence of the circuit breakers during startup. When the charging or discharging mode begins, the startup control circuit closes circuit breakers 1 and 4. The voltage across the high-voltage capacitor, V_{D1}, increases and stabilizes at 270 V causing circuit breaker 2 to operate. Then, the control system starts to regulate V_{D1} to
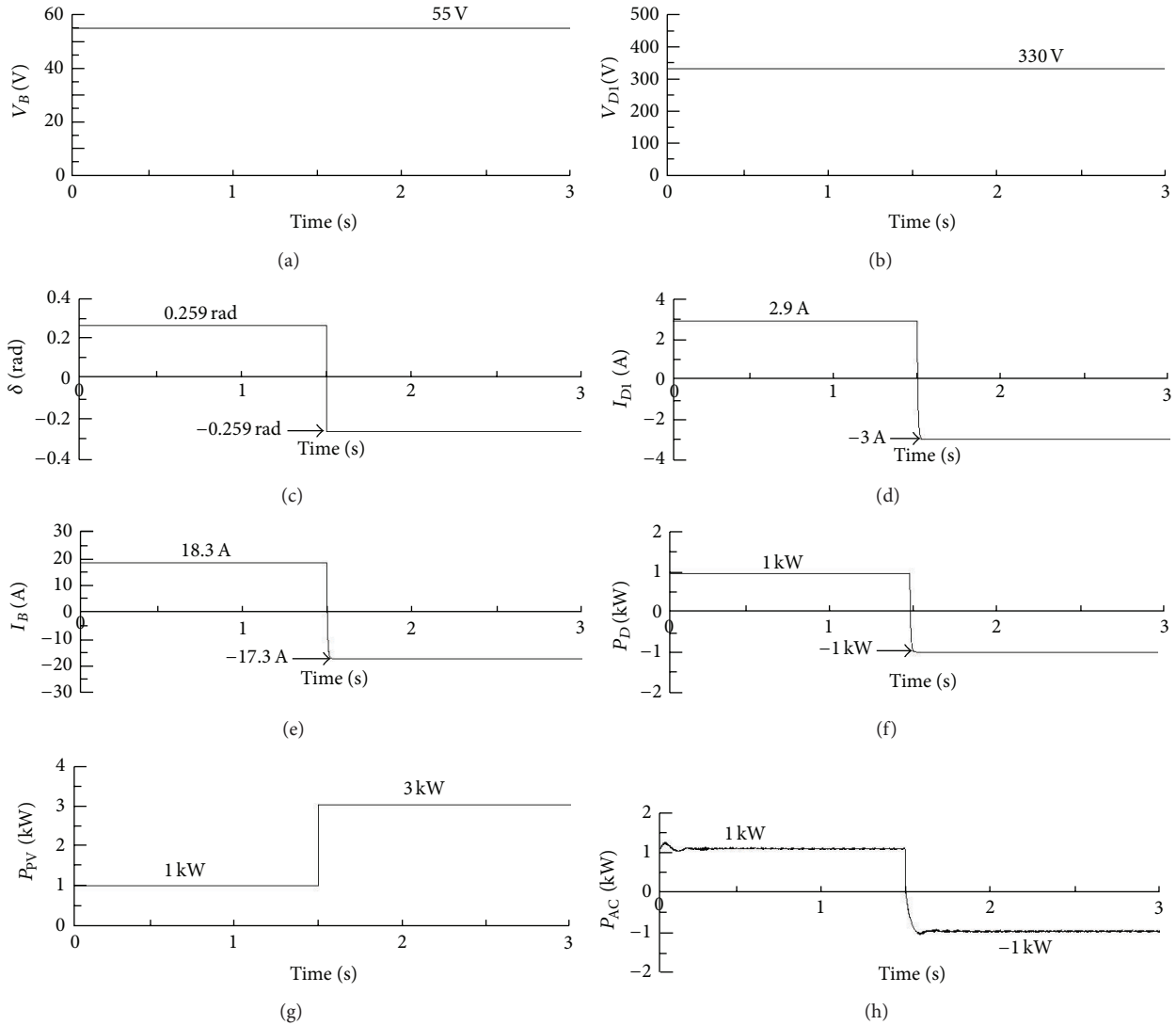
FIGURE 12: Simulation waveforms of the step PV output change from 1 kW to 3 kW. (a) Battery voltage. (b) High voltage side capacitor voltage. (c) Phase shift angle. (d) High-side dc current. (e) Battery current. (f) BESS DC power. (g) PV output power. (h) BESS AC output power.

360 V, provided that the battery voltage is 60 V. As soon as V_{D1} is adjusted at 360 V, circuit breaker 3 will be closed and the BESS will operate as per the requirement of the system.

4. Simulation Waveforms

Figure 8 illustrates the battery voltage at 60 V, 55 V, and 50 V. Figure 9 shows that the capacitor voltage V_{D1} is regulated to 360 V, 330 V, and 300 V to correspond to the change in the battery voltage. The initial voltage of V_{D1} is 270 V because of the start-up sequence. The total duration for the start-up sequence to charge V_{D1} from 0 to 270 V is 1.17 s. The start-up sequence only occurs once at the beginning. When the BESS is in the standby mode, no start-up sequence is required.

Figure 10 illustrates the operation of the BESS with varying PV output power. The simulation assumes that the battery voltage is constant at 60 V and subsequently voltage V_{D1} is regulated at 360 V by operation of the control system.

The output power of P_{PV} is 2 kW at $t = 0$ s. The BESS start-up circuit operates and the voltage of HVS capacitor is regulated to 360 V in 1.17 s. Therefore, the output power from the BESS is equal to zero in this period. At $t = 1.17$ s $P_{PV} = 1$ kW, phase-shift angle δ is increased from 0 to 0.214 rad, so that $P_D = 1$ kW to mitigate the power at the P_{PCC} to 2 kW. At $t = 2$ s, the PV is not injecting any power and phase-shift angle is increased to 0.469 rad. Therefore, the BESS transfers 2 kW to the PCC.

Figure 11 illustrates the operation of the BESS during changes of the solar output power. Four step changes have been employed. The battery voltage is assumed to be constant at 55 V. The BESS provides 1 kW from $t = 0$ s to $t = 1$ s. The BESS transfers 2 kW from $t = 1$ s to $t = 2$ s, between $t = 2$ s and $t = 3$ s, it transfers 1.5 kW, and between $t = 3$ s and $t = 4$ s it provides 1 kW to level the PV output power at the PCC.

Figure 12 presents the operation of the BESS during both charging and discharging modes. The simulation assumes
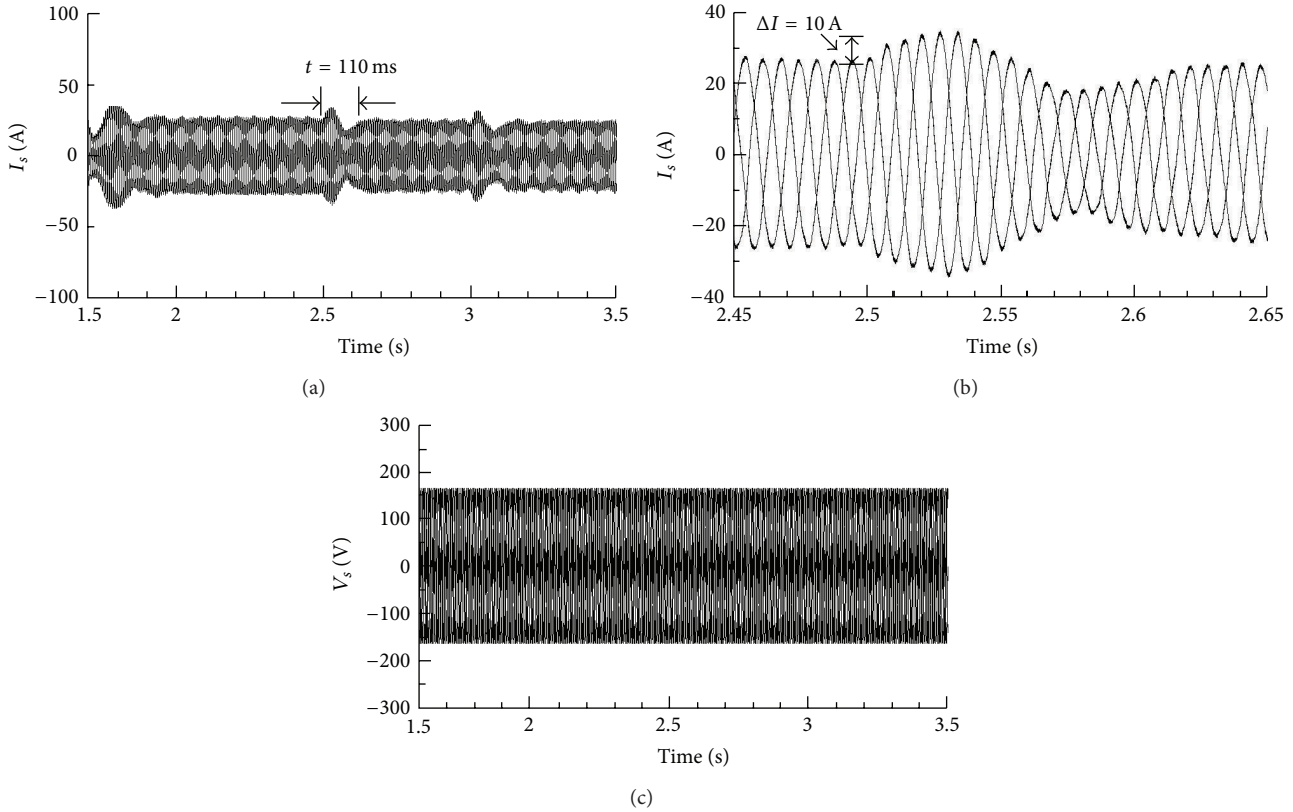
(a)

(b)

(c)

FIGURE 13: (a) Three-phase AC current. (b) Enlarged waveform of the three-phase AC current during a transient condition. (c) Three-phase AC voltage.
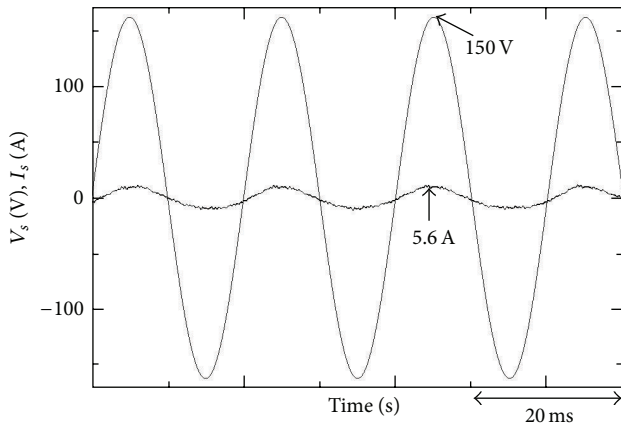

FIGURE 14: AC voltage and current of phase A during the operation of the BESS.

that the battery voltage is constant at 55 V. Between $t = 0$ s and $t = 1.5$ s, the PV is producing $P_{PV} = 1$ kW. The controller of the BESS detects the power which is less than 2 kW. Therefore, the BESS operates to discharge the battery by changing δ from 0 to 0.259 rad, so that the BESS discharges power of 1 kW and mitigates the power at the P_{PCC} to 2 kW. Between $t = 1.5$ s and $t = 3$ s, the output of PV increases to 3 kW. In this mode, the control system detects the output of PV that exceeded

2 kW and battery voltage which is less than 60 V. Therefore, it changes the direction of power and charges the battery bank. So that $P_D = -1$ kW to mitigate the power at the P_{PCC} to 2 kW. When the battery voltage is 60 V, the BESS will go on standby mode.

Figure 13(a) presents the three phase AC current during the operation of the control system. Figure 13(b) shows the transient of the AC current. The transient lasted for 110 ms and the peak of the transient current is 10 A. Figure 13(c) shows the AC output voltage of the BESS. The THD of voltage during charging of the C_{D1} is around 0.7% and during the discharging operation of the dc-dc converter the THD it is negligible.

Figure 14 shows the AC voltage and AC current during the operation of the BESS at the rated power 2 kW and battery voltage 60 V. The synchronized voltage and current waveforms show that the power factor is unity. As explained in Section 3, the control system converges I_q to zero. Therefore, the system works with unity power factor.

Figure 15 shows the AC voltage and current waveforms at the HVS and LVS of the transformer when the power transfer is changed from 1 kW to 2 kW. There are changes to the phase-shift angles from 0.214 rad to 0.504 rad during the change in power transfer requirement. The input and output voltages of transformer are close to the transformer turns ratio. Figure 15(c) shows flat top current. It reduces the rate of change of currents I_1 and I_2 over the time interval
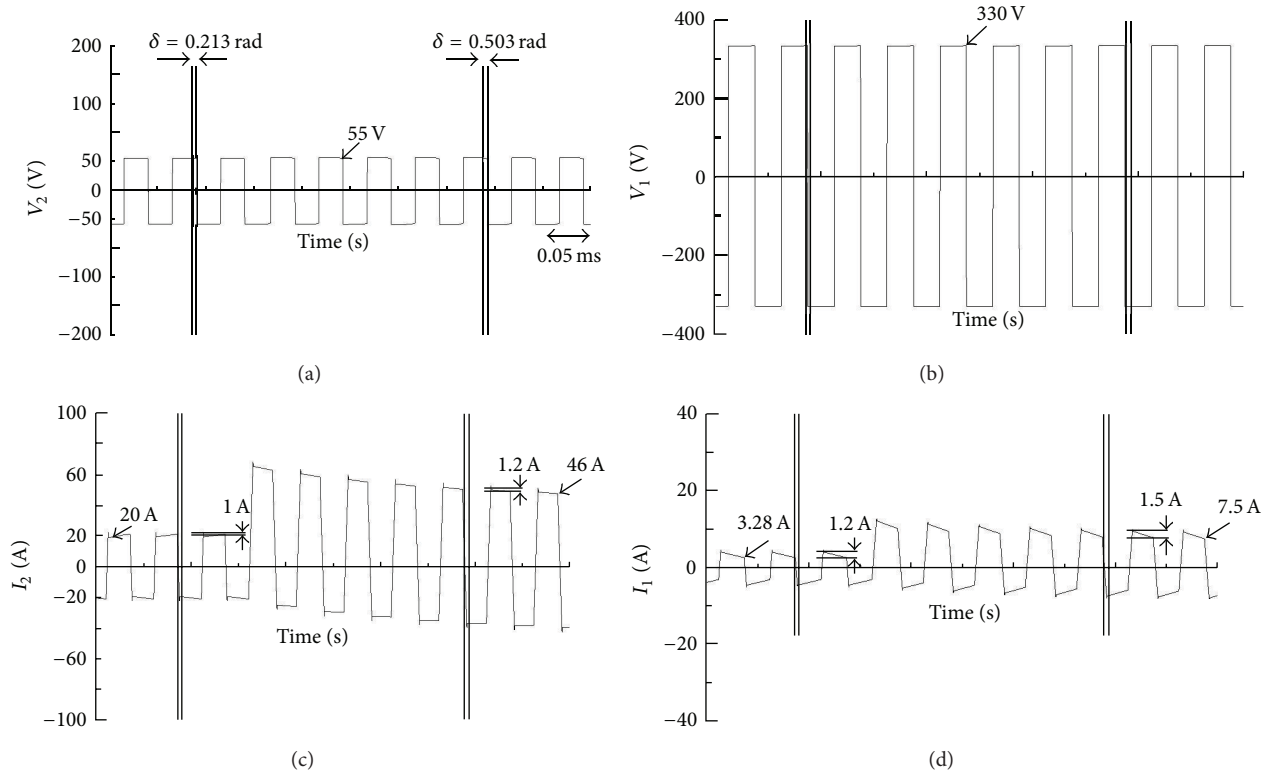
(a)

(b)

(c)

(d)

FIGURE 15: Operation of the phase shift controller during changing power from 1 kW to 2 kW at $V_2 = 55$ V and $V_1 = 330$ V for a duration of 1.7 s. (a) Low-side transformer voltage. (b) High-side transformer voltage side voltage. (c) Low-voltage-side current. (d) High-voltage-side current.

of conduction. Thus, this will minimize the peak switching current which causes a higher switch turn-off overvoltage and improve converter efficiency.

5. Conclusion

The proposed controller that regulates the HVS dc-link capacitor voltage is successful in ensuring that the voltage ratio between the HVS and LVS is close to the transformer turns ratio. This strategy increases the efficiency of the system by minimising the switching current in the dc-dc converter. Unity power factor is also achieved during battery charging and discharging at the utility side. The feasibility of the controller in injecting the required power at the PCC to level the PV output power has been verified via simulation.

Conflict of Interests

The authors declare that there is no conflict of interests regarding the publication of this paper.

References

[1] S. C. Smith, P. K. Sen, and B. Kroposki, "Advancement of energy storage devices and applications in electrical power system," in *Proceedings of the IEEE Power and Energy Society General Meeting: Conversion and Delivery of Electrical Energy in the 21st Century (PES '08)*, pp. 1–8, Pittsburgh, Pa, USA, July 2008.

[2] M. Datta, T. Senjyu, A. Yona, and T. Funabashi, "Photovoltaic output power fluctuations smoothing by selecting optimal capacity of battery for a photovoltaic-diesel hybrid system," *Electric Power Components and Systems*, vol. 39, no. 7, pp. 621–644, 2011.

[3] N. H. Samrat, N. B. Ahmad, I. A. Choudhury, and Z. B. Taha, "Modeling, control, and simulation of battery storage photovoltaic-wave energy hybrid renewable power generation systems for island electrification in malaysia," *Scientific World Journal*, vol. 2014, Article ID 436376, 21 pages, 2014.

[4] A. Solanki, L. F. Montoya, Q. Fu et al., "Managing intermittent renewables in a microgrid," in *Proceedings of the IEEE PES Innovative Smart Grid Technologies (ISGT '12)*, pp. 1–6, January 2012.

[5] A. Nadkarni, G. G. Karady, and K. Alteneder, "Investigation of lithium-ion battery cycling in a grid-tied rooftop PV system through accelerated testing," in *Proceedings of the IEEE PES Innovative Smart Grid Technologies Conference (ISGT '13)*, pp. 1–6, February 2013.

[6] N. M. L. Tan, T. Abe, and H. Akagi, "Topology and application of bidirectional isolated dc-dc converters," in *Proceedings of the 8th International Conference on Power Electronics—ECCE Asia:*

"Green World with Power Electronics" (ICPE-ECCE '11), pp. 1039–1046, Jeju Island, Republic of Korea, June 2011.

[7] R. L. Steigerwald, R. W. de Doncker, and M. H. Kheraluwala, "Comparison of high power DC-to-DC soft-switched converter topologies," in *Proceedings of the 29th IAS Annual Meeting*, pp. 1090–1096, October 1994.

[8] H. Tao, A. Kotsopoulos, J. L. Duarte, and M. A. M. Hendrix, "Transformer-coupled multiport ZVS bidirectional DC-DC converter with wide input range," *IEEE Transactions on Power Electronics*, vol. 23, no. 2, pp. 771–781, 2008.

[9] C. Zhao, S. D. Round, and J. W. Kolar, "An isolated three-port bidirectional dc-dc converter with decoupled power flow management," *IEEE Transactions on Power Electronics*, vol. 23, no. 5, pp. 2443–2453, 2008.

[10] N. M. L. Tan, T. Abe, and H. Akagi, "A 6-kW, 2-kWh lithium-ion battery energy storage system using a bidirectional isolated dc-dc converter," in *Proceedings of the International Power Electronics Conference (IPEC '10)*, pp. 46–52, June 2010.

[11] N. M. L. Tan, T. Abe, and H. Akagi, "Design and performance of a bidirectional isolated DC-DC converter for a battery energy storage system," *IEEE Transactions on Power Electronics*, vol. 27, no. 3, pp. 1237–1248, 2012.

[12] R. W. de Doncker, D. M. Divan, and M. H. Kheraluwala, "A three-phase soft-switched high-power-density DC/DC converter for high-power applications," *IEEE Transactions on Industry Applications*, vol. 27, no. 1, pp. 63–73, 1991.

[13] K. Ravichandrudu, S. Fathima, M. P. Y. Babu, and M. G. Anjaneyulu, "Design and performance of a bidirectional isolated Dc-Dc converter for renewable power system," *Journal of Electrical and Electronics Engineering*, vol. 7, pp. 81–87, 2013.

[14] N. Mendis, K. M. Muttaqi, S. Sayeef, and S. Perera, "Application of a hybrid energy storage in a remote area power supply system," in *Proceedings of the IEEE International Energy Conference and Exhibition (EnergyCon '10)*, pp. 576–581, December 2010.

Journal of
Engineering

The Scientific
World Journal

International Journal of
Rotating
Machinery

Journal of
Sensors

International Journal of
Distributed
Sensor Networks

Advances in
Civil Engineering

Journal of
Control Science
and Engineering

Journal of
Robotics

Hindawi

Submit your manuscripts at
http://www.hindawi.com

Journal of
Electrical and Computer
Engineering

Advances in
OptoElectronics

VLSI Design

International Journal of
Navigation and
Observation

Modelling &
Simulation
in Engineering

International Journal of
Aerospace
Engineering

International Journal of
Chemical Engineering

International Journal of
Antennas and
Propagation

Active and Passive
Electronic Components

Shock and Vibration

Advances in
Acoustics and Vibration